Submitted to ADVANCED ENERGY MATERIALS

DOI: 10.1002/ ((please add manuscript number))
Article type: Full Paper

Interface Modification by Ionic Liquid: A Promising Candidate for Indoor Light Harvesting and Stability Improvement of Planar Perovskite Solar Cells

Meng Li, Chao Zhao, Zhao-Kui Wang, Cong-Cong Zhang, Harrison K. H. Lee, Jeremy Barbe, Wing C. Tsoi, Ying-Guo Yang, Adam Pockett, Matt Carnie, Xing-Yu Gao, Wen-Xing Yang, James R. Durrant, Liang-Sheng Liao*, and S. M. Jain**

M. Li, Dr. Z. K. Wang, C. C. Zhang, Prof. L. S. Liao
Jiangsu Key Laboratory for Carbon-Based Functional Materials & Devices,
Institute of Functional Nano & Soft Materials (FUNSOM),
Soochow University,
Suzhou 215123, China
E-mail: zkwang@suda.edu.cn; lsliao@suda.edu.cn

Dr. C. Zhao, Dr. H. K. H. Lee, Dr. J. Barbe, Dr. W. C. Tsoi, Dr. A. Pockett, Dr. M. Carnie, Dr. S. M. Jain
SPECIFIC, College of Engineering,
Swansea University Bay Campus,
Fabian Way, SA1 8EN Swansea, United Kingdom
E-mail: s.m.jain@swansea.ac.uk, sagarmjain@gmail.com

W. X. Yang, Prof. J. R. Durrant
Department of Chemistry,
Imperial College London,
SW7 2AZ London, United Kingdom

Dr. Y. G. Yang, Prof. X. Y. Gao
Shanghai Synchrotron Radiation Facility,
Shanghai Institute of Applied Physics, Chinese Academy of Sciences,
Shanghai 201204, China

Keywords: Perovskite solar cells; Interface modification; Indoor light; Ionic liquid.

Abstract:

Organic-inorganic hybrid perovskite solar cells (PSCs) are currently attracting significant interest owing to their promising outdoor performance. However, the ability of indoor light harvesting of the perovskites and corresponding device performance are rarely reported. Here, we investigate the potential of planar PSCs in harvesting indoor light for low-power consumption devices. Ionic liquid of 1-butyl-3-methylimidazolium tetrafluoroborate

([BMIM]BF_4) is employed as a modification layer of [6,6]-phenyl-C61-butyric acid methyl ester) (PCBM) in the inverted PSCs. The incorporation of [BMIM]BF_4 not only paves the interface contact between PCBM and electrode, but also facilitates the electron transport and extraction owing to the efficient passivation of the surface trap states. Moreover, [BMIM]BF_4 with excellent thermal stability can act as a protective layer by preventing the erosion of moisture and oxygen into the perovskite layer. The resulting devices present a record indoor power conversion efficiency (PCE) of 35.20% under fluorescent lamps of 1000 lux, and an impressive PCE of 19.30% under 1 sun illumination. The finding in this work verifies the excellent indoor performance of PSCs to meet the requirements of eco-friendly economy.

1. Introduction

In a very short time span, the power conversion efficiency (PCE) of organic-inorganic hybrid perovskite solar cells (PSCs) designed for outdoor application have been approached over 22%.[1,2] Noticeably, very few studies have been reported regarding their potential to indoor applications for low power consumption wireless electronics such as internet of things (IOT) and self-sustainable smart housing.[3-5] Prior to mesoscopic structure, planar device architecture is currently widely employed to fabricate high-performance PSCs by its merits of low-temperature and solution-processing.[6] In a planar PSC, hole- and/or electron-transporting layers are always introduced to manipulate the carrier behaviour in the device. Particularly, a suitable interfacial layer can boost the indoor photovoltaic performance by improving the carrier extraction and reducing the sheet resistance effectively.[3-5] In addition to the tailoring role of the energy levels, the upper interfacial film can also act as a significant protecting layer for the perovskite layer. With a suitable upper interfacial layer, it is prone to retard the infiltration of moisture and oxygen, resulting in a slow-down of the perovskite

decomposition. For example, bathocuproine (BCP) is commonly used as an buffer layer in the inverted planar PSCs.[1,7-19] additionaly, BCP functions as hole blocking layer due to it deep valence band. However, unfortunately BCP suffers from poor film formation with inhomogeneous morphology due to its easy recrystallization. Recently, ionic liquids (ILs) have attracted much attention as ideal candidates for replacing of traditional organic semiconductors owing to their advantages of low volatility, high ion conductivity, and excellent thermal stability.[17-20] Particularly, alteration of the anions or the length of alkyl groups allows a fine tuning of the physicochemical properties of ILs, which enable them deliver wide application in batteries,[20-22] capacitors,[23-25] fuel cells,[26, 27] and photovoltaics [28-33]. For examples, some ILs with unique physicochemical properties have been utilized as the interfacial layers in organic solar cells and PSCs.[30,34,35] The noctorious problem of halide migration in PSCs results in formation of a net positive charge on the crystal surface. photogenerated charge, leading to an increased charge recombination. ILs are ideal candidates for modification of electron transport layers for PSCs. The [BMIM]BF_4 contains

It should be noted that the BCP molecule contains nitrogen atoms with lone pairs and can be considered as an electron-rich molecule. Therefore, the electronrich BCP molecule may have an effect of passivating the surface trap states of perovskite film, similar to those reported aminofunctionalized materials or other electron-rich molecules such as thiophene and pyridine [37]–[39].

However, no studies on fabricating PSCs by utilizing IL as an interface layer to improve the indoor performance are reported so far to the best of our knowledge.

Herein, we demonstrated an efficient interface modification at the cathode side to fabricate the indoor high-performance PSCs by inserting a solution-processed IL layer, named as 1-butyl-3-methylimidazolium tetrafluoroborate ([BMIM]BF_4), between phenyl-C61-butyric

acid methyl ester (PCBM) and silver (Ag) cathode. For comparison, PSCs with three different electron-transporting layers of PCBM, PCBM/BCP, and PCBM/[BMIM]BF_4 were systematically investigated to evaluate the modification role of [BMIM]BF_4 in improving the indoor and outdoor performance of $CH_3NH_3PbI_3$-based PSCs. Transient photovoltage and trap density of states (*t*DOS) measurements revealed that the incorporation of [BMIM]BF_4 not only paved an ideal (or an improved) interface contact between PCBM and Ag electrode, but also facilitated the electron transport and extraction owing to the efficient passivation effect. The resulting PSCs reached a PCE of 19.30% under standard full sunlight illumination (AM 1.5G). Remarkably, the device presented the record indoor PCEs of 35.20% (active area: 9 mm^2) and 23.16% (active area: 4 cm^2) under artificial lighting of 1000 lux. The evaluations by grazing incidence X-ray diffraction and polarized optical microscopy further clarified the protective role of [BMIM]BF_4 in improving the cell stability.

2. Results and Discussion

To evaluate the role of [BMIM]BF_4 as a modification layer in the working PSCs, planar PSCs with a structure of FTO/NiO_x/$CH_3NH_3PbI_3$/PCBM/[BMIM]BF_4/Ag were fabricated as shown in **Figure 1**a. NiO_x and PCBM were used as the hole- and the electron-transporting layer, respectively. The chemical structure and polarized optical microscopic images of [BMIM]BF_4 and BCP are shown in **Figure 1**b. The optical microscope image of the BCP layer showed obvious crystallization behaviour with generated agglomerates at room temperature, whereas the [BMIM]BF_4 film presented a homogeneous coverage without any crystallization. **Figure 1**c gives a cross-sectional scanning electron microscope (SEM) image of the [BMIM]BF_4-based PSCs.

2.1 Modification Effect of [BMIM]BF_4

Figure 2a shows the UV-vis absorption spectra of the $CH_3NH_3PbI_3$ films covered by PCBM, PCBM/BCP and PCBM/[BMIM]BF_4 ETLs. Except slight increases in the spectral range of 400-450 nm after spin-coating ETLs, there was no obvious change in the absorption spectra of the three samples. Steady state photoluminescence (PL) and photovoltage decay measurements were further carried out to evaluate the effects of different ETLs on the transport properties. All samples were excited with a wavelength at 550 nm. As shown in **Figure 2**b, the perovskite layer deposited on glass showed the strongest PL intensity, reflecting a good quality of perovskite films used in this study.[36,37] The PL intensity showed a sequential reduction when depositing PCBM, PCBM/BCP and PCBM/[BMIM]BF_4 on the perovskite layer. Particularly, the sample of $CH_3NH_3PbI_3$/PCBM/[BMIM]BF_4 exhibited the lowest PL intensity, implying the best electron extraction offered by PCBM/[BMIM]BF_4 interfaces.

To further understand the passivation effect of [BMIM]BF_4, a combination measurement of transient photocurrent (TPC) and transient photovoltage (TPV) was carried out on BCP- and [BMIM]BF_4-based PSCs. The pseudo-first-order carrier lifetime carrier lifetime (τ), which corresponds to an average of all potential recombination mechanisms across the entire device,[38,39] was determined by fitting the TPV curves. The differential capacitance (DC) was used to calculate the charge carrier density.[40] As observed from **Figures 2**c and **2**d, the τ value showed an obvious increment at the same carrier density when replacing of BCP by [BMIM]BF_4. We ascribed it to the reduction of recombination rate owing to the better trap passivation by PCBM/[BMIM]BF_4. Furthermore, thermal admittance spectroscopy measurements were further carried out to evaluate the extrinsic trap sites and defect energy distribution in BCP- and [BMIM]BF_4-based PSCs.[41,42] As shown in Figure **2**e, the trap density of state (*t*DOS) in [BMIM]BF_4-based PSC was reduced at the shallow trap region of 0.25~0.45 eV compared to the BCP-based device. This is a direct evidence of the passivation

effect caused by the homogeneous distribution of $[BMIM]BF_4$ layer. Generally, the traps on the perovskite surface and at the grain boundaries can be filled by the solution-processed PCBM or fullerene derivative layer.[43,44] However, the PCBM layer suffers from pinholes which could not be covered by the BCP layer due to its rapid crystallization. In fact, BCP is prone to aggregate with small domains on the surface of the PCBM layer, resulting in the formation of a non-uniform film with poor coverage. In contrast, $[BMIM]BF_4$ can cover the PCBM layer uniformly owing to the absence of crystallization. This results in an efficient filling of the PCBM pinholes and the passivation of defect states. **Figure 2**f illustrates a schematic of the different passivation effects by BCP and $[BMIM]BF_4$.

2.2 Photovoltaic Performance

PSCs with a structure of FTO/NiO_x/$MAPbI_3$/PCBM/modification layer/Ag were fabricated to investigate the effect of different modification layer on the cell performance. The solution concentrations of $[BMIM]BF_4$ (0.8 mg ml^{-1} in ethanol) and BCP (0.5 mg ml^{-1} in ethanol) were determined by the measurements of device efficiency, respectively (Supporting Information, Figures S1, S2 and Tables S1, S2). **Figure 3**a shows the *J-V* characteristics of the PSCs without modification layer, and with either $[BMIM]BF_4$ or BCP modification layer under AM 1.5G illumination (100 mW cm^{-2}). The corresponding photovoltaic parameters of short circuit current density (J_{SC}), open circuit voltage (V_{OC}), fill factor (FF) and PCE are summarized in **Table 1**. Among the three devices, $[BMIM]BF_4$-based cell exhibited the best performance with a PCE of 19.30%, J_{SC} of 23.52 mA cm^{-2}, V_{OC} of 1.06 V, and FF of 77.58%. Compared to the reference device without any modification layer, no large change in V_{OC} was observed. Noticeably, FF and J_{SC} were improved from 69.78% to 77.58% and from 22.42 mA cm^{-2} to 23.52 mA cm^{-2}, respectively.[45] **Figure 3**b shows the performance statistics of over 30 BCP- and $[BMIM]BF_4$-based PSCs. From the PCE histograms, the $[BMIM]BF_4$-based devices

presented an obvious increase in PCE comparted with the BCP-based ones. Device stability of the [BMIM]BF_4-based PSCs was further confirmed by monitoring the steady-state photocurrent and efficiency measured at the maximum power point (0.87 V). As shown in **Figure 3**c, the PCE of the [BMIM]BF_4-based device was finally stabilized at 19.13%, which was close to the value obtained from the reverse scan *J-V* curve. The incident-photon-to-current efficiency (IPCE) spectra of BCP- and [BMIM]BF_4-based devices are displayed in **Figure 3**d. There was no significant change in the photoelectron conversion spectra between the two devices. The integrated photocurrent densities from the IPCE spectra of BCP- and [BMIM]BF_4-based PSCs were 21.31 mA cm^{-2} and 21.75 mA cm^{-2}, respectively, which were agreed well with the J_{SC} values obtained from the corresponding *J-V* curves.

Interestingly, [BMIM]BF_4-based PSCs also presented excellent indoor performance. **Figure 3**e shows the indoor *J-V* curves of the different modification layer based PSCs under 1000 lux irradiation. The corresponding key parameters of J_{SC}, V_{OC}, FF and PCE are presented in **Table 1**. Under low light (1000 lux) illumination, [BMIM]BF_4-based PSC delivered a breakthrough PCE of 35.20%, which was remarkably higher than that (29.44%) of BCP-based device. We ascribed the improved indoor performance to the reduced traps and defects by [BMIM]BF_4 as the *t*DOS results shown in **Figure 2**e. Compared to the stable [BMIM]BF_4, easy crystallization and aggregation of the BCP molecules hindered the carrier collections (low carrier concentration, high recombination rate) under low light. Furthermore, the forward and reverse scanning of *J-V* curves revealed that the [BMIM]BF_4 modification layer could suppress the current hysteresis to some extent (Supporting Information, Figure S3 and Table S3). In addition, [BMIM]BF_4-based devices also exhibited good performance under even lower light intensity such as PCE of 25.7% under 500 lux and PCE of 19.5% under 100 lux (Supporting Information, Figure S4 and Table S4). To investigate the potential application in large-scale, PSCs with an active area of 4 cm^2 were fabricated. As shown in **Figure 3**f and

Table 1, [BMIM]BF_4-based devices shows the best performance with a champion PCE of 23.16% under 1000 lux irradiation, indicating the promising indoor potential for [BMIM]BF_4-based PSCs.

2.3 Cell Stability

Cell stability is a critical factor in determining the practical application of PSCs. To evaluate the protective role of [BMIM]BF_4 in the device stability, the degradation tests of the different modification layer based PSCs without encapsulation were carried out under N_2 atmosphere at various temperatures. At room temperature, the three devices demonstrated similar degradation trend (Supporting Information, Figure S5). After 190 h degradation, all devices still remained approximately half of their original PCEs. At 50 °C, the protective role of [BMIM]BF_4 in the cell stability was observed (Supporting Information, Figure S6). After 50 h, [BMIM]BF_4-based device gradually demonstrated a suppressed degradation behaviour compared to the BCP-based one. **Figure 4**a shows the PCEs in the BCP- and [BMIM]BF_4-based PSCs as a function of time at 80 °C. The PCE of the [BMIM]BF_4-based device still remained 73% of the initial value even after 95 h storage, whereas it reduced to 45% of the initial value for the BCP-based device due to the simultaneous reduction in V_{OC}, J_{SC} and FF (Supporting Information, Figure S7). This means that [BMIM]BF_4 actually could act as a protective layer to prevent the erosion of moisture and oxygen into the perovskite layer by its higher thermal stability. **Figures 4**b and **4**c present the XRD patterns of the fresh and the aged (190 h) $CH_3NH_3PbI_3$ films covered by different modification layers. The fresh perovskite films demonstrated almost the same crystal characteristics regardless of PCBM/[BMIM]BF_4 or PCBM/BCP covering. After 190 h aging, PCBM/BCP-covered perovskite film displayed an additional peak corresponding to PbI_2, implying a partial decomposition of $CH_3NH_3PbI_3$ due to the invasion of moisture and oxygen. In contrast, PCBM/[BMIM]BF_4-covered

perovskite film maintained good stability with pure phase $CH_3NH_3PbI_3$. Two-dimensional grazing incidence X-ray diffraction (GIXRD) was further utilized to study the degradation process of perovskite films. A schematic of perovskite decomposition detected by GIXRD is illustrated in **Figure 4**d. By using the current photon energy of 10 keV, the penetration depth of the X-rays from several nanometres up to tens of micrometres could be realized via varying the incidence angle. From the 2D GIXRD profiles as shown in **Figures 4**e and **4**f, an obvious PbI_2 phase appeared after two weeks aging. In contrast, no PbI_2 peak was observed in the aged sample of $CH_3NH_3PbI_3$/PCBM/$[BMIM]BF_4$. This further confirms the effective protective role of $[BMIM]BF_4$ in resisting the erosion from moisture and oxygen.

To better understand the origin of protective role of $[BMIM]BF_4$ layer, polarized optical microscopic images of BCP and $[BMIM]BF_4$ films were evaluated by varying the aging time. BCP and $[BMIM]BF_4$ films were deposited on glass substrates directly to investigate their aging behaviour. **Figures 5**a-e and **5**f-j show the polarized optical microscope images of BCP and $[BMIM]BF_4$ films, respectively, with varied degradation time from 0 to 420 s in air. Since the amorphous nature of small molecules, BCP film is prone to crystallize and aggregate. As shown in **Figures 5**a-e, the aggregation was observed from 90 s aging and a large number of clusters were formed after 420 s, resulting in numerous pinholes and voids on the surface of BCP films. This means that the aggregated BCP film would open some direct path for the infiltration of moisture and oxygen towards underlying perovskite layer, giving rise to the partial decomposition of perovskite films. In addition, the electron-transporting ability of BCP film would also be negatively affected due to its aggregation behaviour. This could explain the poor stability and low efficiency in the BCP-based PSCs. In contrast, $[BMIM]BF_4$ film kept the excellent stability even after 420 s aging in air. The outstanding chemical and thermal stability as well indoor and outdoor performance enable $[BMIM]BF_4$ act as an excellent interfacial and protective layer in thin film PSCs.

One can observe a large difference in the performance for the PSCs made employing high passivating [BMIM]BF_4 buffer layer in comparison to PSCs made using inhomogeneous BCP layer. This can be related to the direct passivation of larger halide ion migration caused by [BMIM]BF_4 layer expected under illumination and thus passivation of back- and front contact recombination as well as possible trap state healing under operation.

3. Conclusion

We have demonstrated a low-temperature and solution-processable ionic liquid, 1-butyl-3-methylimidazolium tetrafluoroborate ([BMIM]BF_4), to act as an effective electron modification layer and protective layer for fabricating high-performance indoor and outdoor PSCs. The resulting champion device based on $CH_3NH_3PbI_3$ delivered an impressive PCE of 19.30% at 1 sun illumination and a record indoor PCE of 35.20% under fluorescent lamp with 1000 lux, which was the highest value reported so far for indoor PSCs. In the direction of upscaling application, the device with an active area of 4 cm^2 also exhibited a remarkable PCE of 23.16% under 1000 lux. The outstanding performance was attributed to the paving role of interfacial contact and the passivating function of trap states owing to the incorporation of [BMIM]BF_4 modification layer. And the good chemical and thermal stability of [BMIM]BF_4 enable it act as an excellent protective layer by preventing the infiltration of moisture and oxygen into the perovskite layer. The developed modification layer of [BMIM]BF_4 offers a new strategy to fabricate highly efficient and stable PSCs for indoor (self-sustainable electronics) as well as outdoor applications.

4. Experimental Section

Materials and Solution Preparations: Methylamine (24 mL, 33 wt% in absolute ethanol), hydroiodic acid (10 mL, 57 wt% in water), 1-butyl-3-methylimidazolium tetrafluoroborate

([BMIM]BF_4) were purchased from Sigma-Aldrich. Lead iodide (PbI_2, 99.999%), dimethyl sulfoxide, γ-butyrolactone and chlorobenzene were obtained from Alfa Aesar Ltd. CH_3NH_3I was purchased from YOUXUAN Technology Co. Ltd (China). Phenyl-C61-butyric acid methyl ester (PCBM) and BCP were purchased from Nichem Fine Technology Co. Ltd (Taiwan). NiO_x precursor was prepared by dissolving nickel acetate tetrahydrate powder (50 mg) (99.99%, Sigma-Aldrich) into 2-methoxyethanol (1 ml) (99.5%, Sigma-Aldrich) solution with monoethanolamine (12 μl) (Sigma-Aldrich) as a stabilizing agent to improve the solubility of the precursor. Perovskite precursor solution was prepared by mixing 1 mol PbI_2 and 1 mol CH_3NH_3I powder with a molar ration of 1:1 in 1 mL γ-butyrolactone and dimethylsulphoxide (7:3, v/v) with stirring overnight at 60 °C.

Device Fabrication: The FTO substrates with a sheet resistance of ~15 Ω/sq were thoroughly cleaned with acetone, ethanol, and deionized water for sequence in ultrasonic bath for 15 min, respectively. NiO_x solution was then spin-coated onto the FTO substrates under 3000 rpm for 40 s, followed by annealing at 400 °C for 60 min in air. Subsequently, the perovskite solution was then spin-coated onto the NiO_x layer by a consecutive two-step spin-coating process at 1000 and 4000 rpm for 20 and 40 s, respectively, in nitrogen glove box. During the second spin-coating step, the substrate was treated with a chlorobenzene drop-casting, followed by an annealing at 100 °C for 10 min. After annealing, PCBM (20 mg ml^{-1} in chlorobenzene), and modification layer of BCP (in ethanol) or [BMIM]BF_4 (in ethanol) were coated subsequently with a room temperature annealing. Finally, the device was transferred to a vacuum chamber for Ag electrode evaporation under 2×10^{-6} Torr. The PSCs with active area of 9 mm^2 and 4 cm^2 were defined through a shadow mask.

Characterization: The *J-V* characteristics of perovskite solar cells under 1 sun illumination or 100 lux, 500 lux, 1000 lux fluorescent lamps were performed using a programmable Keithley 2400 source meter. Morphologies of BCP and [BMIM]BF_4 were characterized using a

polarized optical microscope (Leica, DM4000M). The grazing incidence X-ray diffraction (GIXRD) measurements were performed at the BL14B1 beamline of the Shanghai Synchrotron Radiation Facility (SSRF) using X-ray with a wavelength of 1.24 Å. Two-dimensional (2D) GIXRD patterns were acquired by a MarCCD mounted vertically at a distance ~223 mm from the sample with a grazing incidence angle of 0.2° and an exposure time of 20 s. The 2D GIXRD patterns were analyzed using the FIT2D software and displayed in scattering vector q coordinates. The energetics and recombination kinetics of the PSCs were investigated by differential charging (DC) method which is a combination of transient photovoltage (TPV) and transient photocurrent (TPC) measurements. TPV and TPC were performed using a transient measurement system (Automatic Research GmbH) with an oscilloscope (Keysight DSOX2024A) as the data capture (The details can be seen in Supporting Information).

Supporting Information

Supporting Information is available from the Wiley Online Library or from the authors.

Acknowledgements

M. L. and C. Z. contributed equally to this work. The authors acknowledge financial support from the Natural Science Foundation of China (Nos. 91733301, 61674109), the National Key R&D Program of China (No. 2016YFA0202400), and the Natural Science Foundation of Jiangsu Province (No.BK20170059). This project is also funded by the Collaborative Innovation Center of Suzhou Nano Science and Technology, by the Priority Academic Program Development of Jiangsu Higher Education Institutions (PAPD), and by the "111" Project of The State Administration of Foreign Experts Affairs of China. S. M. J.

acknowledge Marie Curie COFUND fellowship, Welsh Assembly Government funded Ser-Cymru Solar Project and the Swedish research council (VR) for the financial supports. C.Z. A.P. and M.J.C. also thank for Welsh European Funding Office (SPARC II). This project has received funding from the European Union's Horizon 2020 research and innovation programme under the Marie Skłodowska Curie grant agreement (No. 663830).

Received: ((will be filled in by the editorial staff))
Revised: ((will be filled in by the editorial staff))
Published online: ((will be filled in by the editorial staff))

References

1. Z. Wei, H. Chen, K. Yan, X. Zheng, S. Yang, *J. Mater. Chem. A* **2015**, *3*, 24226.
2. Y. Rong, Y. Hu, S. Ravishankar, H. Liu, X. Hou, Y. Sheng, A. Mei, Q. Wang, D. Li, M. Xu, J. Bisquert, H. Han, *Energy Environ. Sci.* **2017**, *10*, 2383.
3. H. K. H. Lee, Z. Li, J. R. Durrant, W. C. Tsoi, *Appl. Phys. Lett.* **2016**, *108*, 253301.
4. R. Steim, T. Ameri, P. Schilinsky, C. Waldauf, G. Dennler, M. Scharber, C. J. Brabec, *Sol. Energy Mater. Sol. Cells* **2011**, *95*, 3256.
5. H. K. H. Lee, J. Wu, J. Barbe, S. M. Jain, S. Wood, E. M. Speller, Z. Li, F. A. Castro, J. R. Durrant, W. C. Tsoi, *J. Mater. Chem. A* **2018**, *6*, 5618.
6. M. Li, Z. K. Wang, M. P. Zhuo, Y. Hu, K. H. Hu, Q. Q. Ye, S. M. Jain, Y. G. Yang, X. Y. Gao, L. S. Liao, *Adv. Mater.* **2018**, *30*, 1800258.
7. Y. Tu, J. Wu, Z. Lan, X. He, J. Dong, J. Jia, P. Guo, J. Lin, M. Huang, Y. Huang, *Sci. Rep.* **2017**, *7*, 44603.
8. J.-Y. Jeng, Y.-F. Chiang, M.-H. Lee, S.-R. Peng, T.-F. Guo, P. Chen, T.-C. Wen, *Adv. Mater.* **2013**, *25*, 3727.
9. J.-Y. Jeng, K.-C. Chen, T.-Y. Chiang, P.-Y. Lin, T.-D. Tsai, Y.-C. Chang, T.-F. Guo, P. Chen, T.-C. Wen, Y.-J. Hsu, *Adv. Mater.* **2014**, *26*, 4107.

10. J. Seo, S. Park, Y. Chan Kim, N. J. Jeon, J. H. Noh, S. C. Yoon, S. I. Seok, *Energy Environ. Sci.* **2014**, *7*, 2642.
11. Q. Wang, Y. Shao, Q. Dong, Z. Xiao, Y. Yuan, J. Huang, *Energy Environ. Sci.* **2014**, *7*, 2359.
12. X. Liu, H. Yu, L. Yan, Q. Dong, Q. Wan, Y. Zhou, B. Song, Y. Li, *ACS Appl. Mater. & Inter.* **2015**, *7*, 6230.
13. C. Bi, Y. Yuan, Y. Fang, J. Huang, *Adv. Energy Mater* **2015**, *5*, 1401616.
14. J. H. Heo, H. J. Han, D. Kim, T. K. Ahn, S. H. Im, *Energy Environ. Sci.* **2015**, *8*, 1602.
15. J. Cui, F. Meng, H. Zhang, K. Cao, H. Yuan, Y. Cheng, F. Huang, M. Wang, *ACS Appl. Mater. & Inter.* **2014**, *6*, 22862.
16. A. K. Jena, H.-W. Chen, A. Kogo, Y. Sanehira, M. Ikegami, T. Miyasaka, *ACS Appl. Mater. & Inter.* **2015**, *7*, 9817.
17. Z. Zhu, Y. Bai, T. Zhang, Z. Liu, X. Long, Z. Wei, Z. Wang, L. Zhang, J. Wang, F. Yan, S. Yang, *Angew. Chem.* **2014**, *126*, 12779.
18. Y. Hu, Z. Zhang, A. Mei, Y. Jiang, X. Hou, Q. Wang, K. Du, Y. Rong, Y. Zhou, G. Xu, H. Han, *Adv. Mater.* **2018**, *30*, 1705786.
19. Y. Hu, S. Si, A. Mei, Y. Rong, H. Liu, X. Li, H. Han, *Solar RRL* **2017**, *1*, 1600019.
20. D. R. MacFarlane, P. Meakin, J. Sun, N. Amini, M. Forsyth, *J. Phys. Chem. B* **1999**, *103*, 4164.
21. H. Sakaebe, H. Matsumoto, *Electrochem. Commun.* **2003**, *5*, 594.
22. J.-H. Shin, W. A. Henderson, S. Passerini, *J. Electrochem. Soc.* **2005**, *152*, A978.
23. M. Ue, M. Takeda, A. Toriumi, A. Kominato, R. Hagiwara, Y. Ito, *J. Electrochem. Soc.* **2003**, *150*, A499.
24. S. A. Hashmi, R. J. Latham, R. G. Linford, W. S. Schlindwein, *J. Chem. Soc.* **1997**, *93*, 4177.
25. A. Matsuda, H. Honjo, M. Tatsumisago, T. Minami, *Solid State Ionics* **1998**, *113*, 97.
26. R. F. de Souza, J. C. Padilha, R. S. Gonçalves, J. Dupont, *Electrochem. Commun.* **2003**, *5*, 728.
27. M. Guo, J. Fang, H. Xu, W. Li, X. Lu, C. Lan, K. Li, *J. Membr. Sci.* **2010**, *362*, 97.
28. F. Fabregat-Santiago, J. Bisquert, E. Palomares, L. Otero, D. Kuang, S. M. Zakeeruddin, M. Grätzel, *J. Phys. Chem. C* **2007**, *111*, 6550.
29. D. Kuang, S. Uchida, R. Humphry-Baker, S. M. Zakeeruddin, M. Grätzel, *Angew. Chem.* **2008**, *120*, 1949.

30. J.-Y. Seo, T. Matsui, J. Luo, J.-P. Correa-Baena, F. Giordano, M. Saliba, K. Schenk, A. Ummadisingu, K. Domanski, M. Hadadian, A. Hagfeldt, S. M. Zakeeruddin, U. Steiner, M. Grätzel, A. Abate, *Adv. Energy Mater.* **2016**, *6*, 1600767.
31. J.-D. Decoppet, S. B. Khan, M. S. A. Al-Ghamdi, B. G. Alhogbi, A. M. Asiri, S. M. Zakeeruddin, M. Grätzel, *Energy Technol.* **2017**, *5*, 321.
32. D. T. Moore, K. W. Tan, H. Sai, K. P. Barteau, U. Wiesner, L. A. Estroff, *Chemistry of Materials* **2015**, *27*, 3197.
33. M. Shahiduzzaman, K. Yamamoto, Y. Furumoto, K. Yonezawa, K. Hamada, K. Kuroda, K. Ninomiya, M. Karakawa, T. Kuwabara, K. Takahashi, K. Takahashi, T. Taima, *Org. Elec.* **2017**, *48*, 147.
34. W. Yu, L. Huang, D. Yang, P. Fu, L. Zhou, J. Zhang, C. Li, *J. Mater. Chem. A* **2015**, *3*, 10660.
35. D. Yang, R. Yang, X. Ren, X. Zhu, Z. Yang, C. Li, S. Liu, *Adv. Mater.* **2016**, *28*, 5206.
36. S. M. Jain, B. Philippe, E. M. J. Johansson, B.-w. Park, H. Rensmo, T. Edvinsson, G. Boschloo, *J. Mater. Chem. A* **2016**, *4*, 2630.
37. S. M. Jain, Z. Qiu, L. Haggman, M. Mirmohades, M. B. Johansson, T. Edvinsson, G. Boschloo, *Energy Environ. Sci.* **2016**, *9*, 3770.
38. A. J. Pearson, G. E. Eperon, P. E. Hopkinson, S. N. Habisreutinger, J. T.-W. Wang, H. J. Snaith, N. C. Greenham, *Adv. Energy Mater.* **2016**, *6*, 1600014.
39. D. H. Sin, H. Ko, S. B. Jo, M. Kim, G. Y. Bae, K. Cho, *ACS Appl. Mater. Inter.* **2016**, *8*, 6546.
40. Y. Li, L. Meng, Y. M. Yang, G. Xu, Z. Hong, Q. Chen, J. You, G. Li, Y. Yang, Y. Li, *Nat. Commun.* **2016**, *7*, 10214.
41. C. Bi, X. Zheng, B. Chen, H. Wei, J. Huang, *ACS Energy Lett.* **2017**, *2*, 1400.
42. Y. Shao, Y. Yuan, J. Huang, *Nat. Energy* **2016**, *1*, 15001.
43. X. Liu, F. Lin, C.-C. Chueh, Q. Chen, T. Zhao, P.-W. Liang, Z. Zhu, Y. Sun, A. K. Y. Jen, *Nano Energy* **2016**, *30*, 417.
44. Y. Wu, X. Yang, W. Chen, Y. Yue, M. Cai, F. Xie, E. Bi, A. Islam, L. Han, *Nat. Energy* **2016**, *1*, 16148.
45. G.-H. Kim, H.-B. Kim, B. Walker, H. Choi, C. Yang, J. Park, J. Y. Kim, *ACS Appl. Mater. Inter.* **2013**, *5*, 1757.

Figures and Tables

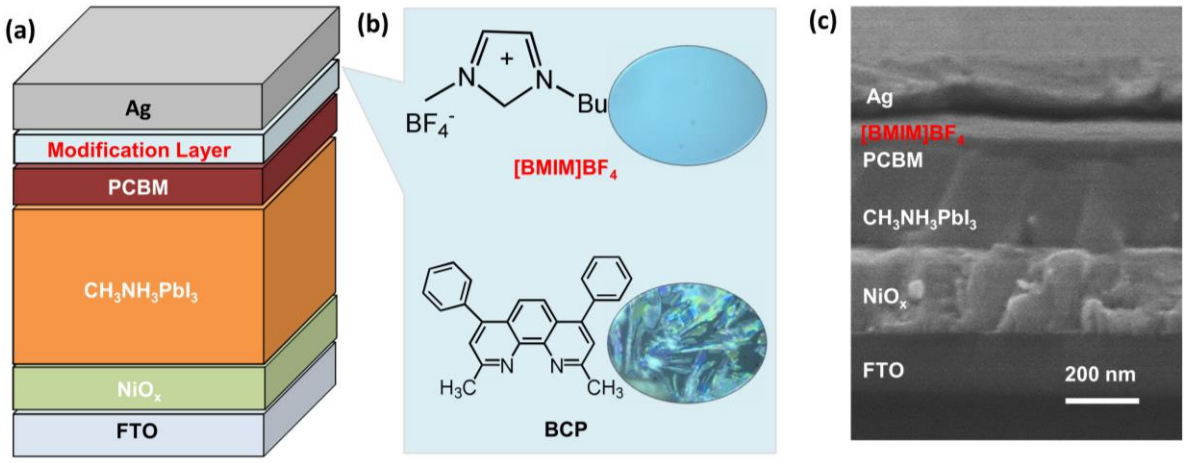

Figure 1. (a) A schematic of inverted p-i-n structure PSCs; (b) Molecule structures of [BMIM]BF_4 and BCP, and corresponding polarized optical microscopic images; (c) The cross-sectional SEM image of the [BMIM]BF_4-based PSCs.

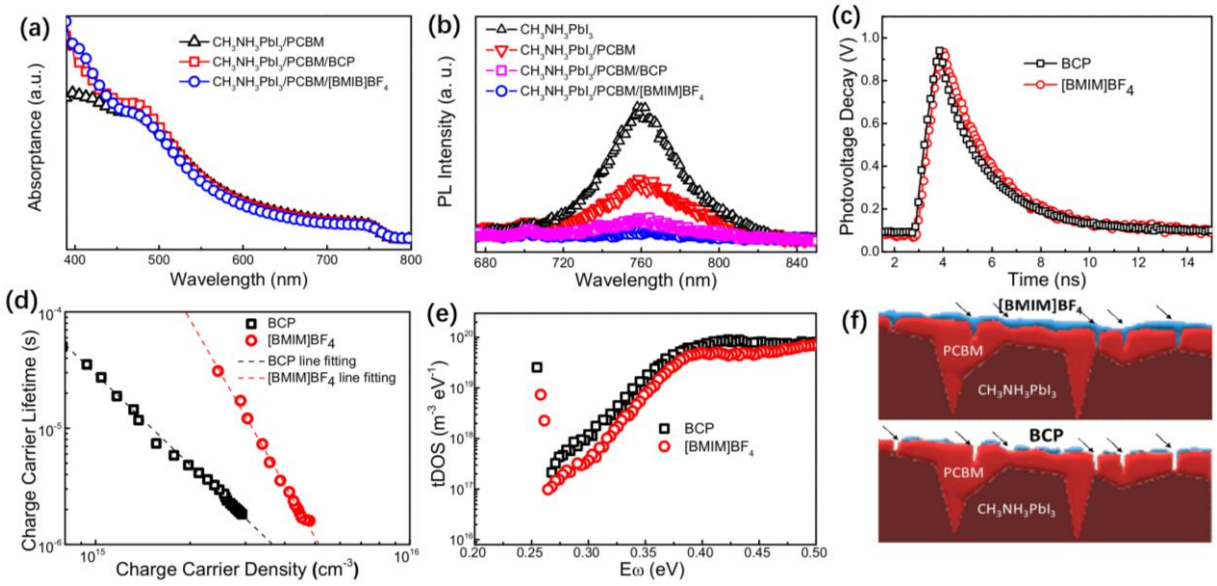

Figure 2. (a) Absorption spectra of $CH_3NH_3PbI_3$ films covered with PCBM, PCBM/BCP and PCBM/[BMIM]BF_4; (b) Steady-state PL spectra of $CH_3NH_3PbI_3$ films covered with PCBM, PCBM/BCP and PCBM/[BMIM]BF_4; (c) Transient photovoltage (TPV) decay in the BCP- and [BMIM]BF_4-based PSCs; (d) Charge carrier lifetimes as a function of charge carrier density in the BCP- and [BMIM]BF_4-based PSCs; (e) Trap density of states (tDOS) in the BCP- and [BMIM]BF_4-based PSCs; (f) A schematic of the different passivation effects by BCP and [BMIM]BF_4.

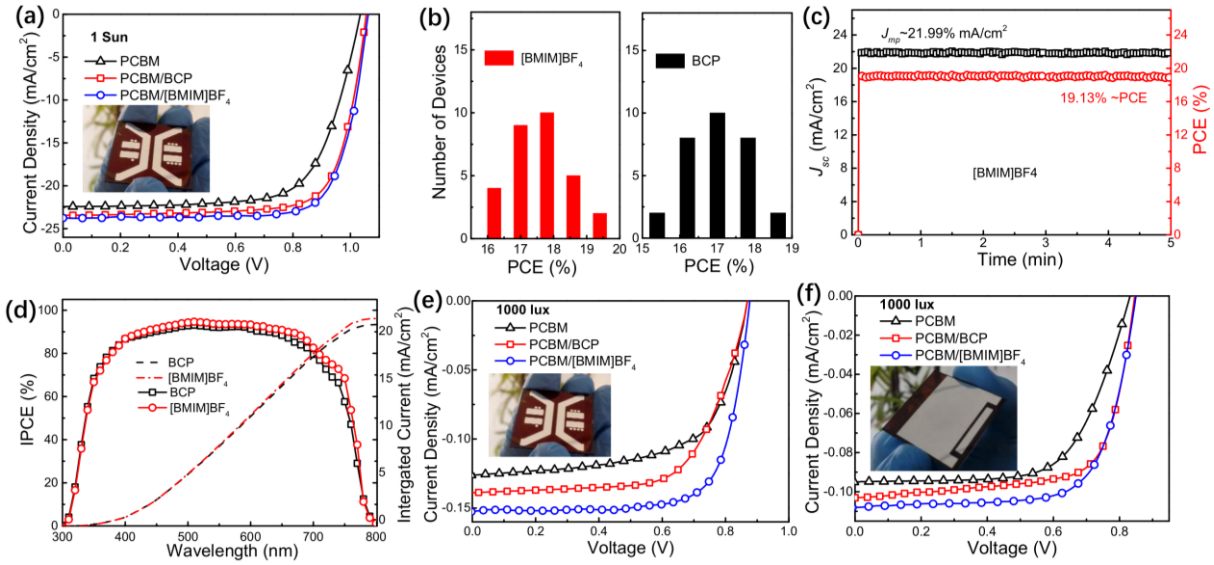

Figure 3. (a) *J-V* curves of champion PSCs (9 mm^2) based on PCBM, PCBM/BCP and PCBM/[BMIM]BF_4 ETLs under AM 1.5G illumination with an intensity of 100 mW cm^{-2}; (b) PCE histograms measured for over 30 BCP- and [BMIM]BF_4-based PSCs; (c) Maximal steady-state photocurrent output at the maximum power point for [BMIM]BF_4-based PSC at 0.87 V and corresponding power output; (d) IPCE spectra of BCP- and [BMIM]BF_4-based PSCs and integrated current densities from the IPCE spectra; (e) *J-V* curves of champion PSCs (9 mm^2) based on PCBM, PCBM/BCP and PCBM/[BMIM]BF_4 ETLs under indoor irradiation of 1000 lux; (f) *J-V* curves of champion PSCs (4 cm^2) based on PCBM, PCBM/BCP and PCBM/[BMIM]BF_4 ETLs under indoor irradiation of 1000 lux.

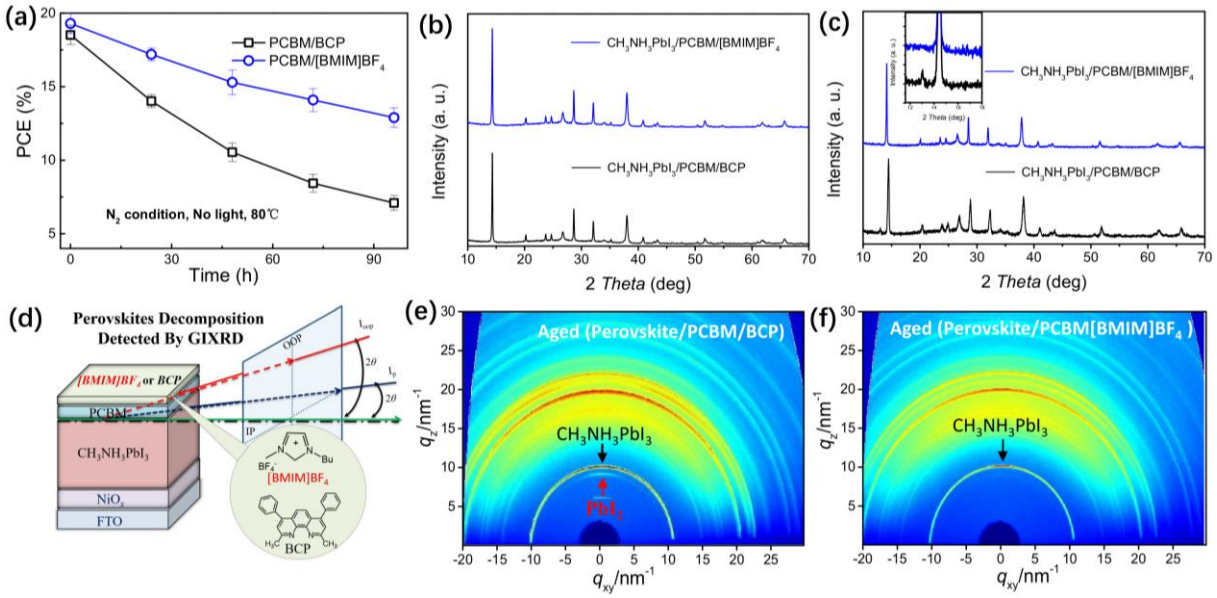

Figure 4. (a) PCE degradations as a function of time in BCP- and $[BMIM]BF_4$-based PSCs without encapsulation under N_2 atmosphere at elevated temperature of 80 ^oC; (b) XRD patterns of fresh $CH_3NH_3PbI_3$ films covered with PCBM/BCP and PCBM/$[BMIM]BF_4$; (c) XRD patterns of aged (190 h) $CH_3NH_3PbI_3$ films covered with PCBM/BCP and PCBM/$[BMIM]BF_4$; (d) A schematic of perovskite decomposition detected by GIXRD technique; 2D GIXRD profiles of aged (336 h) $CH_3NH_3PbI_3$ films covered with (e) PCBM/BCP and (f) PCBM/$[BMIM]BF_4$.

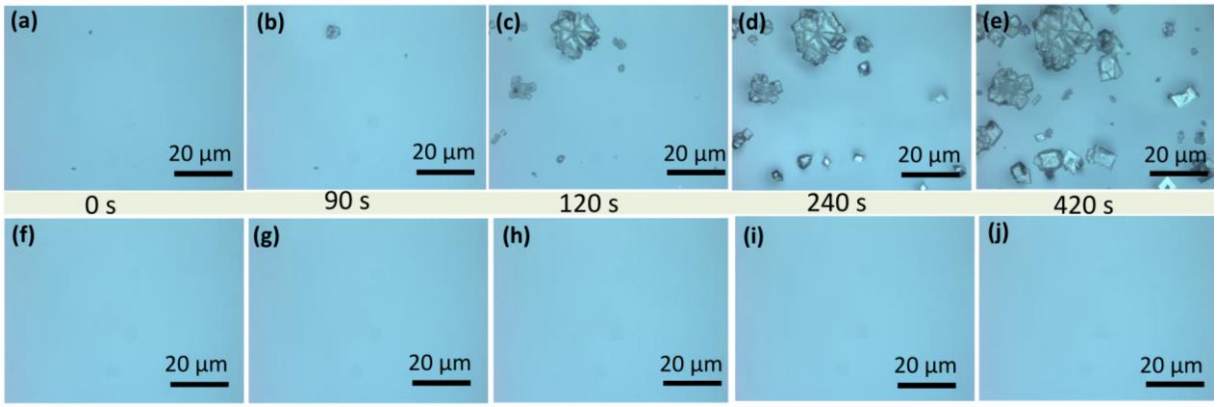

Figure 5. Polarized optical microscopic images of aged (a)-(e) BCP films and (f)-(j) [BMIM]BF_4 films with varied time from 0~420 s.

Table 1. Cell parameters of p-i-n PSCs with different ETLs under various illumination intensity.

Illumination & Device Area	**ETL**	V_{OC} **(V)**	J_{SC} **(mA/cm^2)**	**FF**	**PCE (%)**	**PCE$_{AVE}$ (%)**
1 Sun 9 mm^2	PCBM	1.04	22.42	70	16.24	16.15±0.23
	PCBM/BCP	1.06	23.22	75	18.52	18.24±0.31
	PCBM/[BMIM]BF_4	1.06	23.52	77	19.30	19.09±0.21

1000 lux 9 mm^2	PCBM	0.86	0.126	64	26.25	25.72±0.50
	PCBM/BCP	0.86	0.135	67	29.44	28.89±0.57
	PCBM/[BMIM]BF_4	0.87	0.150	75	35.20	34.62±0.60
1000 lux 4 cm^2	PCBM	0.83	0.095	65	18.65	18.46±0.23
	PCBM/BCP	0.84	0.102	69	21.26	21.14±0.31
	PCBM/[BMIM]BF_4	0.84	0.108	71	23.16	23.06±0.11

Table of Content:

Ionic liquid of 1-butyl-3-methylimidazolium tetrafluoroborate ([BMIM]BF_4) is employed as a cathode modification layer and a protective layer to fabricate indoor perovskite solar cells.

The resulting devices delivered an impressive PCE of 19.30% at 1 sun illumination, and a record indoor PCE of 35.20% under fluorescent lamp with 1000 lux, which was the highest value reported so far for indoor solar cells.

Keywords: Perovskite solar cells; Interface modification; Indoor light; Ionic liquid.

By *Meng Li, Chao Zhao, Zhao-Kui Wang*, Cong-Cong Zhang, Harrison K. H. Lee, Jeremy Barbe, Wing C. Tsoi, Ying-Guo Yang, Adam Pockett, Matt Carnie, Xing-Yu Gao, Wen-Xing Yang, James R. Durrant, Liang-Sheng Liao*, and S. M. Jain**

Title: **Interface Modification by Ionic Liquid: A Promising Candidate for Indoor Light Harvesting and Stability of Planar Perovskite Solar Cells**

ToC figure ((Please choose one size: 55 mm broad × 50 mm high or 110 mm broad × 20 mm high. Please do not use any other dimensions))

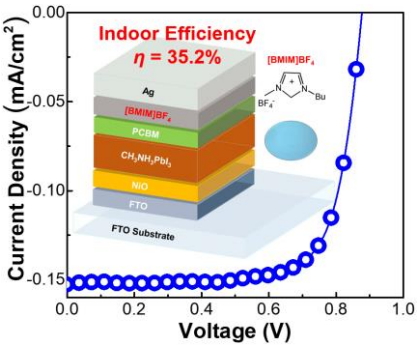

((Supporting Information can be included here using this template))

Supporting Information

Interface Modification by Ionic Liquid: A Promising Candidate for Indoor Light Harvesting and Stability of Planar Perovskite Solar Cells

Meng Li, Chao Zhao, Zhao-Kui Wang, Cong-Cong Zhang, Harrison K. H. Lee, Jeremy Barbe, Wing C. Tsoi, Ying-Guo Yang, Adam Pockett, Matt Carnie, Xing-Yu Gao, Wen-Xing Yang, James R. Durrant, Liang-Sheng Liao*, and S. M. Jain**

M. Li, Dr. Z. K. Wang, C. C. Zhang, Prof. L. S. Liao
Jiangsu Key Laboratory for Carbon-Based Functional Materials & Devices,
Institute of Functional Nano & Soft Materials (FUNSOM),
Soochow University,
Suzhou 215123, China
E-mail: zkwang@suda.edu.cn; lsliao@suda.edu.cn

Dr. C. Zhao, Dr. H. K. H. Lee, Dr. J. Barbe, Dr. W. C. Tsoi, Dr. A. Pockett, Dr. M. Carnie, Dr. S. M. Jain
SPECIFIC, College of Engineering,
Swansea University Bay Campus,
Fabian Way, SA1 8EN Swansea, United Kingdom
E-mail: s.m.jain@swansea.ac.uk, sagarmjain@gmail.com

W. X. Yang, Prof. J. R. Durrant
Department of Chemistry,
Imperial College London,
SW7 2AZ London, United Kingdom

Dr. Y. G. Yang, Prof. X. Y. Gao
Shanghai Synchrotron Radiation Facility,
Shanghai Institute of Applied Physics, Chinese Academy of Sciences,
Shanghai 201204, China

Keywords: Perovskite solar cells; Interface modification; Indoor light; Ionic liquid.

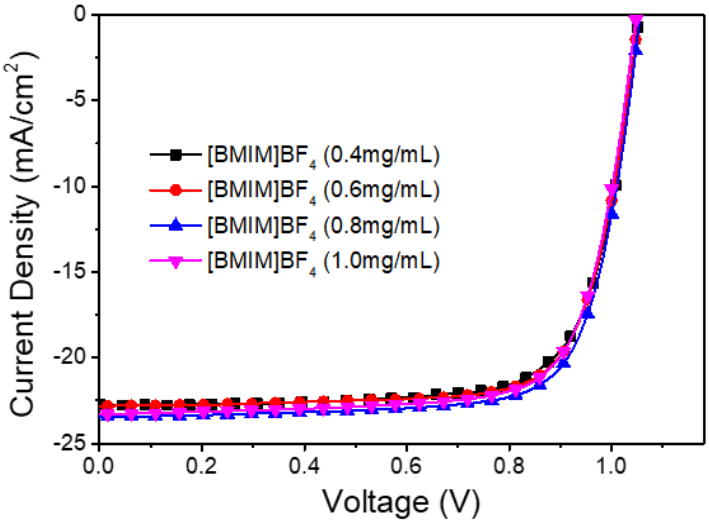

Figure S1. *J-V* curves of [BMIM]BF_4-based PSCs with varied [BMIM]BF_4 concentration in in ethanol.

Table S1. Performance parameters of [BMIM]BF_4-based PSCs.

Device	V_{OC} (V)	J_{SC} (mA/cm^2)	FF (%)	PCE (%)
[BMIM]BF_4 (0.4mg/mL)	1.06	22.77	73.66	17.78
[BMIM]BF_4 (0.6mg/mL)	1.06	22.83	75.01	18.09
[BMIM]BF_4 (0.8mg/mL)	1.06	23.52	77.58	19.30
[BMIM]BF_4 (1.0mg/mL)	1.06	23.30	73.91	18.19

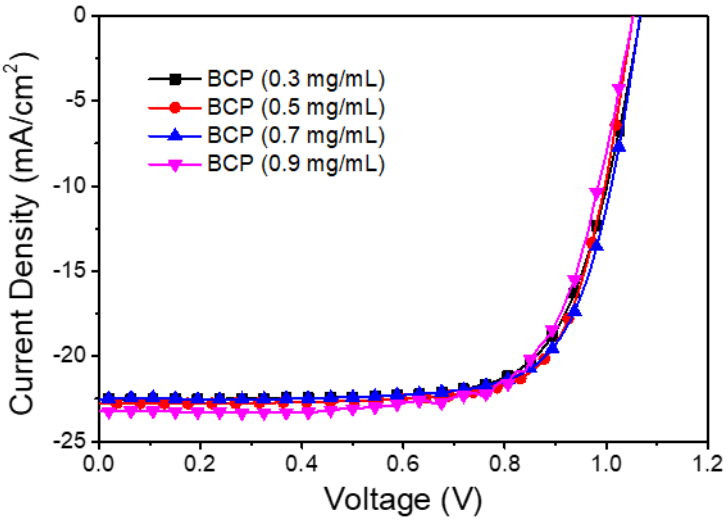

Figure S2. *J-V* curves of BCP-based PSCs with varied BCP concentration in ethanol.

Table S2. Performance parameters in BCP-based PSCs.

Device	V_{OC} (V)	J_{SC} (mA/cm^2)	FF (%)	PCE (%)
BCP (0.3mg/mL)	1.06	22.53	71.25	17.24
BCP (0.5mg/mL)	1.06	23.22	75.24	18.52

BCP (0.7mg/mL)	1.06	23.53	73.26	18.21
BCP (0.9mg/mL)	1.06	23.24	71.13	17.52

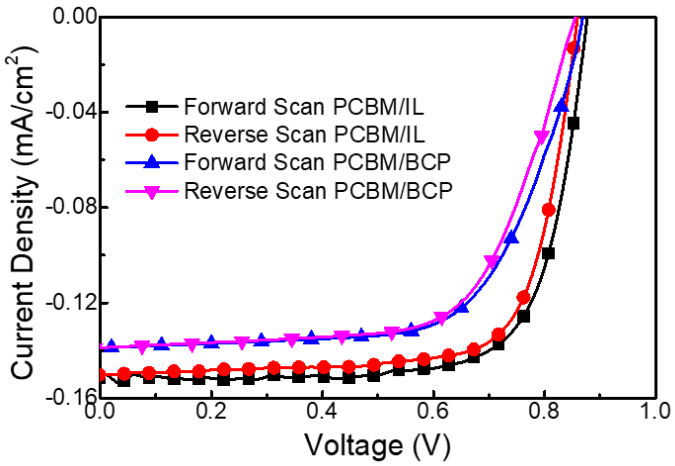

Figure S3. *J-V* curves of BCP- and [BMIM]BF_4 (IL)-based PSCs scanned in forward and reverse directions.

Table S3. Performance parameters in BCP- and [BMIM]BF_4 (IL)-based PSCs.

Device	V_{OC} (V)	J_{SC} (mA/cm^2)	FF (%)	PCE (%)
PCBM/BCP (Forward)	0.86	0.135	67	29.44
PCBM/BCP (Reverse)	0.85	0.135	67	28.94
PCBM/IL (Forward)	0.87	0.150	75	35.20
PCBM/IL (Reverse)	0.85	0.150	75	34.24

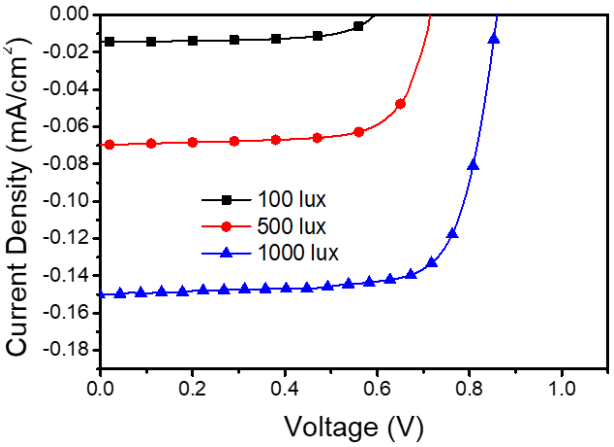

Figure S4. *J-V* curves of [BMIM]BF_4-based PSCs scanned under varied illumination intensity.

Table S4. Performance parameters in [BMIM]BF_4 (IL)-based PSCs under varied intensity.

Illumination Intensity	ETL	V_{OC} (V)	J_{SC} (mA/cm^2)	FF (%)	PCE (%)
100 lux	PCBM/IL	0.58	0.014	66	19.5
500 lux	PCBM/IL	0.69	0.070	74	25.7
1000 lux	PCBM/IL	0.87	0.150	75	35.2

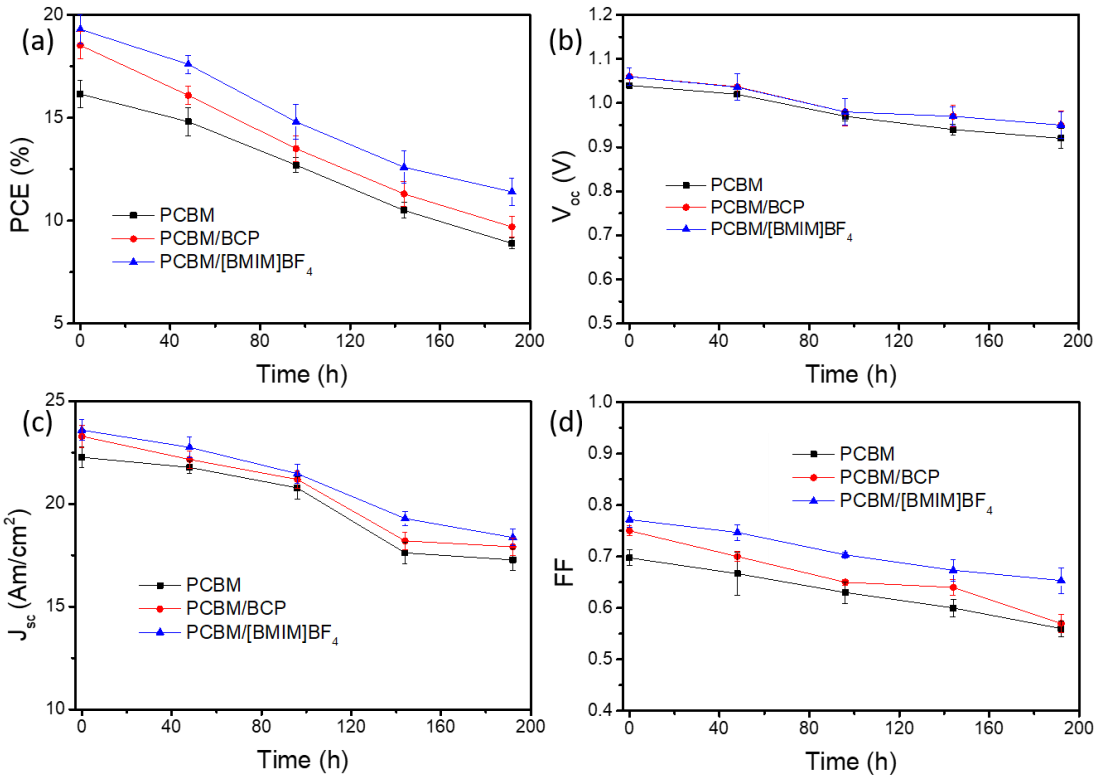

Figure S5. Stability tests of cell parameters a) PCE, b) V_{OC}, c) J_{SC}, and d) FF in PCBM-, PCBM/BCP- and PCBM/[BMIM]BF_4-based PSCs under the N_2 atmosphere at the room temperature.

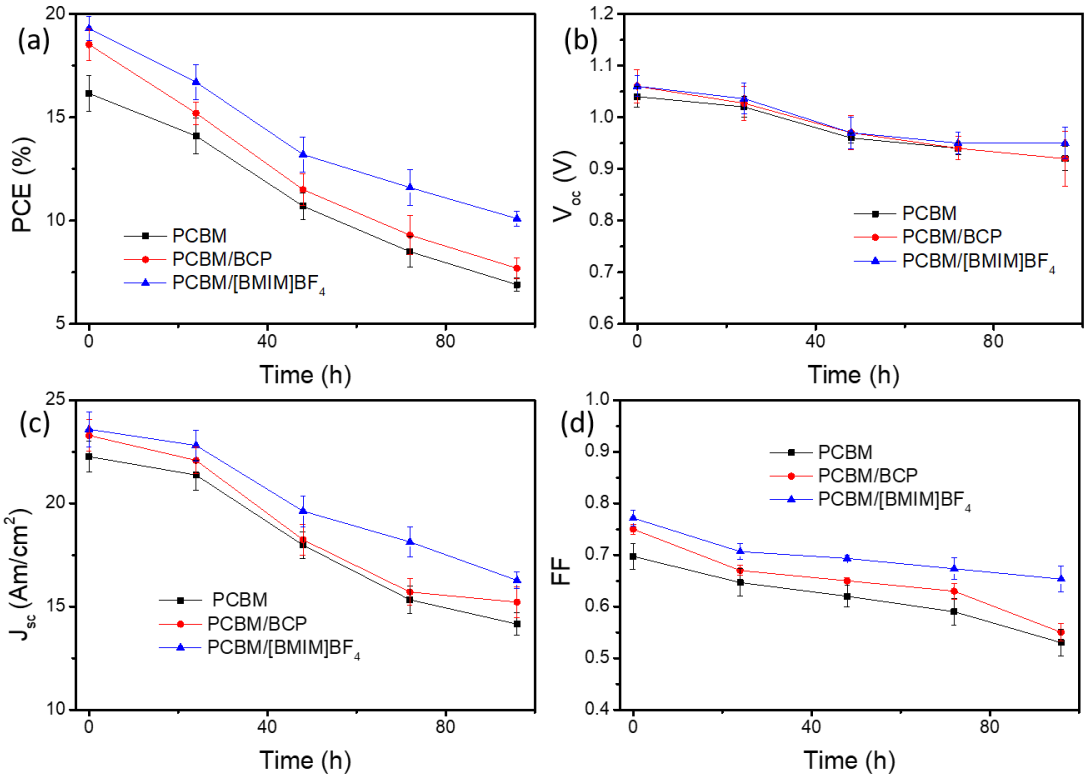
(a)
PCE (%)
Time (h)
PCBM
PCBM/BCP
PCBM/[BMIM]BF4
(b)
Voc (V)
Time (h)
PCBM
PCBM/BCP
PCBM/[BMIM]BF4
(c)
Jsc (Am/cm2)
Time (h)
PCBM
PCBM/BCP
PCBM/[BMIM]BF4
(d)
FF
Time (h)
PCBM
PCBM/BCP
PCBM/[BMIM]BF4

Figure S6. Stability tests of cell parameters a) PCE, b) V_{OC}, c) J_{SC}, and d) FF in PCBM-, PCBM/BCP- and PCBM/[BMIM]BF_4-based PSCs under the N_2 atmosphere at the 50 ^oC.

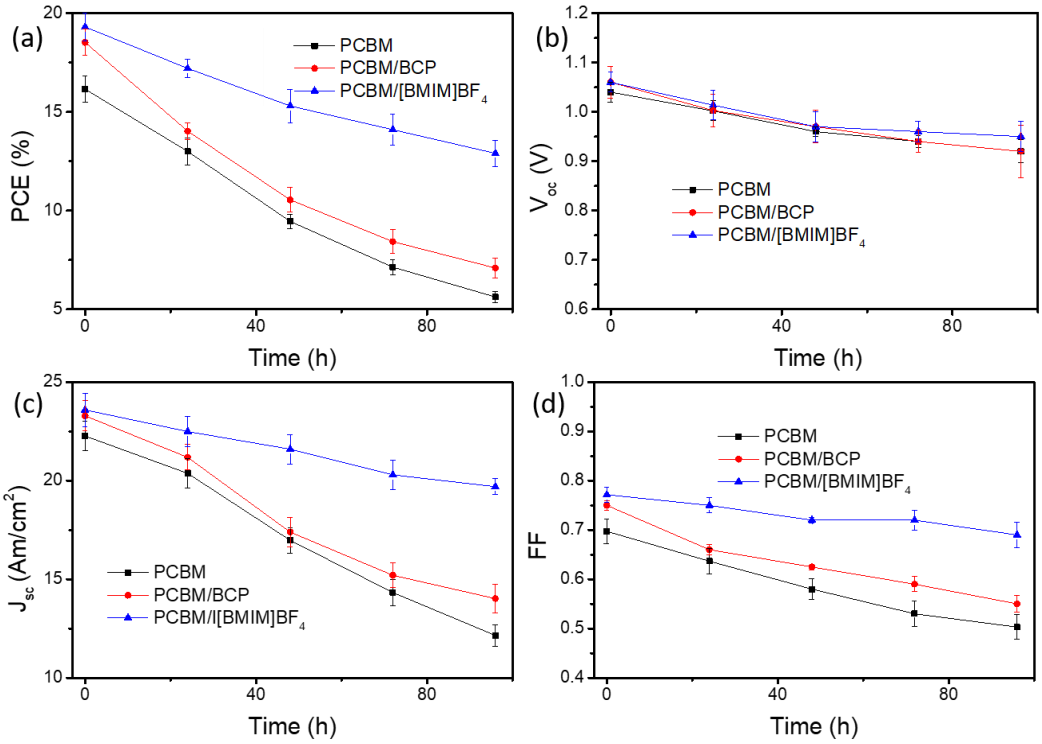

Figure S7. Stability tests of cell parameters a) PCE, b) V_{OC}, c) J_{SC}, and d) FF in PCBM-, PCBM/BCP- and PCBM/[BMIM]BF_4-based PSCs under the N_2 atmosphere at the 80 ^oC.

Measuring Process of TPV and TPC

Transient photovoltage (TPV) and transient photocurrent (TPC) were performed using a transient measurement system (Automatic Research GmbH) with an oscilloscope (Keysight DSOX2024A) as the data capture. The system used a waveform generator (Keysight 33500B) to control the green laser diode which could general a controllable laser pulse (typically with length between 10 to 500 μs) to study different features of the transient response. An intensity calibrated white LED was employed to support the background illumination and maintain the device generate equal photocurrent as measured using the solar simulator. Each measurement was performed several times for optimizing signal noise and measurement time. For the TPV measurements, the PSCs were held at open-circuit by the 1 MΩ oscilloscope input with variable, continuous intensity background illumination. After equilibration (~15 s), the PSCs were perturbed by a single pulse and the resulting voltage transient was recorded. In the case of TPC measurement, the PSCs were held close to short-circuit conditions with a 50 Ω measurement resistance. The current perturbation signal was calculated from the voltage signal measured from the resistant by Ohm's law which had the same excitation as it had been used for TPV measurements. The current result was then integrated to obtain the number of carriers generated by the optical pulse. Steady state emission measurements were done on the Horiba Fluoromax-4 spectroflurometer equipped with double-grating at the excitation wavelength of 550 nm on the 3-layer assembly of Glass/$CH_3NH_3PbI_3$/ETLs (PCBM, PCBM/BCP, and PCBM/[BMIM]BF_4). Front face illumination with respect to the incident beam was used to minimize the inner filter effects. Time Correlated Single Photon Counting

measurements were performed on Horiba Jobin Yvon Fluorolog system. Steady state photoluminescence measurements were done on perovskite and electronic transport layers with < 200 ps pulses of 635 nm excitation from a pisosecond diode laser (NanoLED source). The laser pulse excitation density was $2.3x10^{14}$ cm^{-3} (Rep.rate:1MHz). Measurements were done in reverse mode (Rep. rate: 1 MHz). A cutoff filter (OG575) was used to block the stray excitation light. To increase the sensitivity of measurements, all wavelengths transmitted by cutoff filter were collected without the use of any monochromator.